How to cite: *Angew. Chem. Int. Ed.* **2024**, *63*, e202316200
doi.org/10.1002/anie.202316200

Gold Clusters

Assembly of Luminescent Chiral Gold(I)-Sulfido Clusters via Chiral Self-Sorting

*Liao-Yuan Yao, Lin Qin, Ziyong Chen, Jonathan Lam, and V. W.-W. Yam**

Abstract: Due to the ubiquity of chirality in nature, chiral self-assembly involving self-sorting behaviors has remained as one of the most important research topics of interests. Herein, starting from a racemic mixture of SEG-based (SEG = SEGPHOS) chlorogold(I) precursors, a unique chiral butterfly-shape hexadecanuclear gold(I) cluster (Au_{16}) with different ratios of R^{SEG} and S^{SEG} ligands is obtained via homoleptic and heterochiral self-sorting. More interestingly, by employing different chlorogold(I) precursors of opposite chirality (such as $\boldsymbol{R^{SEG}}$**-Au$_2$** and $\boldsymbol{S^{BIN}}$**-Au$_2$** (BIN = BINAP)), an unprecedented heteroleptic and heterochiral self-sorting strategy has been developed to give a series of heteroleptic chiral decanuclear gold(I) clusters (Au_{10}) with propellor-shape structures. Heterochiral and heteroleptic self-sorting have also been observed between enantiomers of homoleptic chiral Au_{10} clusters to result in the heteroleptic chiral Au_{10} clusters via cluster-to-cluster transformation. Incorporation of heteroleptic ligands is found to decrease the symmetry from S_4 of homoleptic *meso* Au_{10} to C_2 of heteroleptic chiral Au_{10} clusters. The chirality has been transferred from the axial chiral ligands and stored in the heteroleptic gold(I) clusters.

Introduction

Self-assembly involving self-sorting behaviors in chiral systems has attracted continuous research interests,[1–3] because chirality is one of the fundamental features of life systems. Development of artificial processes capable of a control of the handedness and recognition of a certain enantiomer can help to provide an understanding of the origin of chirality and provide insights into processes that occur in nature.[4–7] In artificial systems, chiral self-sorting mostly involves recognition and discrimination between the homoleptic enantiomers to give homochiral or heterochiral assemblies.[8–17] However, in nature, chiral selectivity mainly occurs between different species, such as the production of proteins from L-amino acids using RNA with D-ribose,[18,19] enzyme catalysis between enzyme hosts and specific guests,[20,21] therapeutics using chiral drugs,[22,23] and so on. Therefore, an exploration into chirality-driven self-sorting and an understanding of chiral selectivity behaviors in heteroleptic chiral systems would represent areas of interest and is of vital importance.

Among aurophilicity-supported gold(I) assemblies,[24–61] gold(I) chalcogenido complexes of high stability and synthetic accessibility have attracted considerable attention in recent decades.[27,30–47] Gold(I) cluster species possess diverse configurations and attractive structure-dependent photophysical behavior, showing promises towards luminescence,[26,30–33] catalysis,[37] chemosensing,[34,41,44] self-assembly,[39,43] and so on. Moreover, the dynamic nature of Au(I)···Au(I) (aurophilic) interactions in gold(I) species has contributed to the success of their self-assembly and chiral self-sorting in artificial gold(I) systems.[35,38,39,41–45] The success of aurophilicity-driven self-assembly has prompted chemists to explore the full potential of these features in driving directed assembly strategies.[25,26] Even though both chiral self-sorting and heteroleptic self-sorting have been independently proved to be highly efficient in the fine-control of self-assembly in supramolecular coordination systems,[62–64] to the best of our knowledge, utilization of chiral self-sorting strategy to build novel structures in cluster chemistry has rarely been developed in recent years[65,66] since it is highly challenging to achieve both heterochiral and heteroleptic self-sorting between chemically different components in the cluster system.

Herein, by employing different axial chiral ligands (Scheme 1) derived chlorogold(I) precursors or decanuclear gold(I) (Au_{10}) clusters of opposite chirality, an unprece-

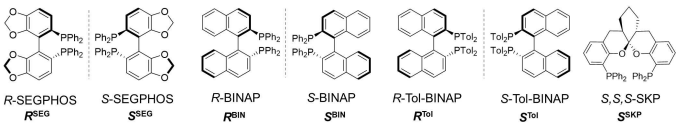

Scheme 1. Axial chiral ligands involved in this work.

[*] Prof. Dr. L.-Y. Yao, Dr. Z. Chen, Dr. J. Lam, Prof. Dr. V. W.-W. Yam
Institute of Molecular Functional Materials, State Key Laboratory of Synthetic Chemistry and Department of Chemistry, The University of Hong Kong
Pokfulam Road, Hong Kong (P. R. China)
E-mail: wwyam@hku.hk
Prof. Dr. L.-Y. Yao, Dr. L. Qin
MOE Key Laboratory of Cluster Sciences, School of Chemistry and Chemical Engineering, Beijing Institute of Technology
8 Liangxiang East Road, Beijing 102488 (P. R. China)

dented heterochiral and heteroleptic self-sorting strategy has been developed to give a series of heteroleptic chiral propellor-shape Au_{10} clusters (Scheme 2). Incorporation of heterochiral and heteroleptic ligands renders the symmetry of the propellor-shape Au_{10} clusters to be lowered from local S_4 of the homoleptic clusters to chiral C_2 of the heteroleptic clusters. Besides, a unique butterfly-shape chiral hexadecanuclear gold(I) (Au_{16}) complex with different ratios of R^{SEG} and S^{SEG} ligands is obtained through heterochiral self-sorting between enantiomers of SEGPHOS-supported chlorogold(I) precursors (SEGPHOS = 5,5′-bis(diphenylphosphino)-4,4′-bi-1,3-benzodioxole). The combinations of the chiral ligands are anticipated to influence the chirality, composition, symmetry, and even Au(I)···Au(I) interactions of the resulting gold(I) complexes, which may lead to structure-dependent photophysical behaviors and circular dichroism (CD) origins.

Results and Discussion

Reaction of the respective enantiopure chiral chlorogold(I) precursors, $[R^{SEG}(AuCl)_2]$ (***R*^SEG^-Au₂**), $[S^{SEG}(AuCl)_2]$ (***S*^SEG^-Au₂**), with Li_2S in CH_2Cl_2 gives the corresponding chiral decanuclear gold(I) clusters, $[Au_{10}(R^{SEG})_4(\mu_3\text{-}S)_4]Cl_2$ (***R*^SEG^-Au₁₀**) and $[Au_{10}(S^{SEG})_4(\mu_3\text{-}S)_4]Cl_2$ (***S*^SEG^-Au₁₀**) (see the Supporting Information). The $^{31}P\{^1H\}$ NMR spectra of these chiral Au_{10} complexes reveal the adoption of a similar structure as BINAP-protected chiral Au_{10} clusters (Figures 1a and S1).[39] Their identities are further established by high-resolution electrospray-ionization mass spectrometry (HR-ESI-MS) (Figures 1b and S2). The m/z value at 2269.56 in Figure 1b is assignable to the cluster dication of $[Au_{10}(SEGPHOS)_4(\mu_3\text{-}S)_4]^{2+}$. The single crystal X-ray diffraction (SCXRD) of ***S*^SEG^-Au₁₀** unambiguously establishes its four-leaf-clover-shape Au_{10} structure (Figure 1c). The Tol-BINAP-protected chiral clusters, $[Au_{10}(R^{Tol})_4(\mu_3\text{-}S)_4]Cl_2$ (***R*^Tol^-Au₁₀**) and $[Au_{10}(S^{Tol})_4(\mu_3\text{-}S)_4]Cl_2$ (***S*^Tol^-Au₁₀**), were similarly

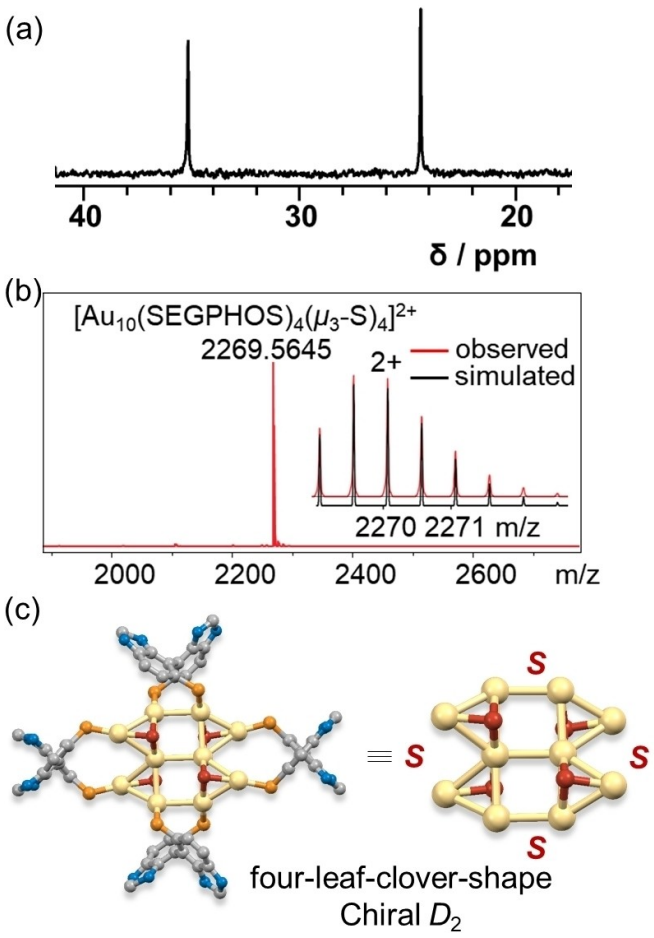

Figure 1. (a) $^{31}P\{^1H\}$ NMR and (b) ESI-TOF mass spectra of ***S*^SEG^-Au₁₀** with the inset showing the observed and simulated isotopic patterns of dicationic cluster ion of Au_{10}. (c) Crystal structure of ***S*^SEG^-Au₁₀** showing the four-leaf-clover-shape structure (left) and the $Au_{10}S_4$ core surrounded by four S^{SEG} ligands (right). (The counteranions, hydrogen atoms, and phenyl rings are omitted for clarity. Au, yellow; S, red; P, orange; C, grey; O, blue.)

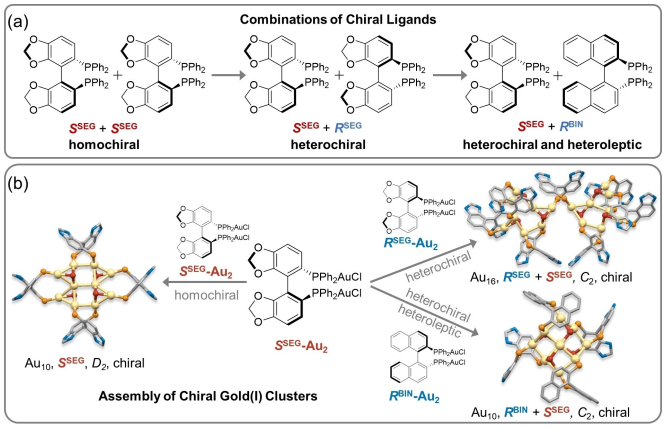

Scheme 2. (a) Evolution of combinations of chiral ligands. (b) Chiral self-assembly from homochiral assembly to heterochiral self-sorting and heterochiral and heteroleptic self-sorting for the construction of new types of chiral polynuclear gold(I) clusters.

synthesized and have been fully characterized (see the Supporting Information, Figures S3 and S4). With the influence of the axial chiral ligands, both these clusters and their $Au_{10}S_4$ cores possess a local chiral D_2 symmetry (Figure 1c).

Surprisingly, reaction of the racemic mixture of ***R*^SEG^-Au₂** and ***S*^SEG^-Au₂** and Li_2S was found to afford pale yellow crystals, which on dissolution in $CDCl_3$, gave rather complicated NMR patterns (Figures 2a and b). In the $^{31}P\{^1H\}$ NMR spectrum, seven sets of signals are observed, indicating seven different phosphorus chemical environments (Figure 2b). The cluster ion observed at m/z values of around 1904.32 in the ESI-mass spectrum corresponds to the molecular formula of $[Au_{16}(SEGHPOS)_7(\mu_3\text{-}S)_6]^{4+}$ (Figure 2c). In sharp contrast, employment of the racemic mixture of ***R*^Tol^-Au₂** and ***S*^Tol^-Au₂** was found to give a propellor-shape *meso* Au_{10} cluster (***meso*^Tol^-Au₁₀**) (see the Supporting Information, Figures S5 and S6), which is

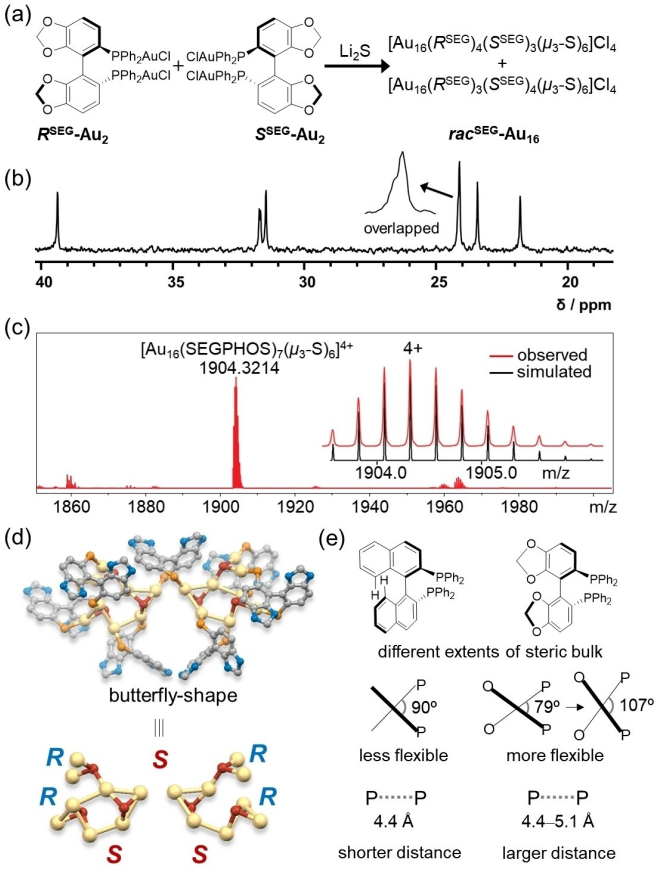

Figure 2. (a) Synthetic route for ***rac*^SEG-Au16**. (b) $^{31}P\{^{1}H\}$ NMR spectrum showing seven different phosphorus chemical environments. (c) ESI-TOF mass spectrum of ***rac*^SEG-Au16** with the inset showing the observed and simulated isotopic patterns of the tetracationic cluster of Au_{16}. (d) Crystal structure of one of the enantiomers of ***rac*^SEG-Au16** and the order of the protecting chiral ligands. (The counter-anions, hydrogen atoms, and phenyl rings are omitted for clarity. Au, yellow; S, red; P, orange; C, grey; O, blue.) (e) Illustration of the relationship between different extents of steric bulk, flexibility and P···P distances.

analogous to the previously reported *meso* Au_{10} with BINAP ligands.[39]

The structure of Au_{16} has been confirmed by SCXRD analysis as $[Au_{16}(R^{SEG})_4(S^{SEG})_3(\mu_3\text{-}S)_6]Cl_4$ or $[Au_{16}(R^{SEG})_3(S^{SEG})_4(\mu_3\text{-}S)_6]Cl_4$ (***rac*^SEG-Au16**), an unprecedented Au_{16} cluster supported by both R^{SEG} and S^{SEG} ligands (Figure 2d). Different from other heterochiral assemblies, the 4:3 or 3:4 ratio of R^{SEG} and S^{SEG} ligands is found in each Au_{16} molecule, giving a chiral Au_{16} complex. In other words, a phenomenon of chiral self-discrimination has occurred between R^{SEG} and S^{SEG} species during the self-assembly of the Au_{16} complex. From the single crystal structure, the Au_{16} cluster crystallizes in a centrosymmetric space group $P2_1/c$ as a racemic mixture and adopts a butterfly-shape structure that can be viewed as two Au_8 motifs linked by a R^{SEG} or S^{SEG} ligand (Figure 2d). To our knowledge, it is the first time to obtain gold(I)-chalcogenido complex of hexadecanuclear cluster core. In addition, it represents the first case to have chiral gold(I) clusters with unequal ratio of ligand enantiomers.

Attempts have been made to figure out why butterfly-shape Au_{16} instead of propellor-shape Au_{10} involving the SEG ligand was obtained. From the X-ray structure, the dihedral angles between the benzodioxole planes of ***rac*^SEG-Au16** are in the range of 78.79–106.65° while that between the naphthalene planes in both ***meso*^BIN-Au10** and ***meso*^Tol-Au10** are almost around 90° (Figure 2e). The higher flexibility between the benzodioxole planes of the SEG ligands gives rise to a more diverse range of dihedral angles than that of the BINAP ligands (Figure 2e). To further confirm the relatively large flexibility of SEGPHOS ligands in gold(I) clusters, the single-point energy for each conformer of ***R*^BIN-Au2** and ***R*^SEG-Au2** precursors (as model complexes) was plotted against the dihedral angles (θ) of the respective benzodioxole planes and naphthalene planes by density functional theory (DFT) calculations (Figure S7). For both complexes, the global energetic minimum was found with a θ of 91.54° for ***R*^BIN-Au2** and 92.87° for ***R*^SEG-Au2**. More significantly, the shape of the potential energy surface differs between ***R*^BIN-Au2** and ***R*^SEG-Au2**: whereas the variation in energy with respect to θ follows a roughly parabolic curve in ***R*^BIN-Au2**, the potential energy surface of ***R*^SEG-Au2** is much flatter in the low-θ region, making the low-θ conformations accessible in the case of ***R*^SEG-Au2** but not in ***R*^BIN-Au2** (Figure S7). This results in the greater flexibility observed in the case of ***R*^SEG-Au2**.

As a result, the P···P distances in the SEGPHOS ligands of ***rac*^SEG-Au16** are from 4.4 to around 5.1 Å, while those in ***meso*^Tol-Au10** are around 4.3–4.4 Å. The different P···P distances have resulted in different Au···Au contacts as well as distinct cluster structures. The dependence of the structure on the P···P distances in diphosphine-protected gold(I)-sulfido clusters has also previously been demonstrated.[35,38,41] It is likely that the different extents of steric bulk will have an impact on the P···P distances and flexibility that determines the formation of such unusual Au_{16} complex.

It is interesting to understand what will happen if the different ligands with opposite chirality are combined for the synthesis of the gold(I)-sulfido clusters. To explore the full potential of chiral self-sorting in this system, a mixture of ***R*^BIN-Au2** and ***S*^SEG-Au2** with equal equivalents is employed as reaction precursor to produce polynuclear gold(I) complexes (Figure 3a). Isolation followed by ESI-MS and SCXRD studies establishes the identity and structure as ***R*^BIN*S*^SEG-Au10** ($[Au_{10}(R^{BIN})_2(S^{SEG})_2(\mu_3\text{-}S)_4]Cl_2$), a novel pseudo *meso* Au_{10} cluster supported by heteroleptic R^{BIN} and S^{SEG} ligands (Figures 3a and b). The enantiomer ***R*^SEG*S*^BIN-Au10** was synthesized and isolated through the same procedures followed by ESI-MS and SCXRD characterizations (Figures S8 and S9). ***R*^BIN*S*^SEG-Au10** crystallizes in chiral space group $P2_12_12$ and the crystal structure clearly shows a propellor-shape Au_{10} cluster supported by alternating R^{BIN} and S^{SEG} ligands ($R^{BIN}S^{SEG}R^{BIN}S^{SEG}$). Since the S_4 symmetry is destroyed by the application of the different ligands (R^{BIN} and S^{SEG}), only local C_2 symmetry is left for ***R*^BIN*S*^SEG-Au10** molecular ion to give an unprecedented chiral heteroleptic Au_{10} cluster (Figure 3c). In other words, heterochiral and heteroleptic self-sorting between the BINAP and

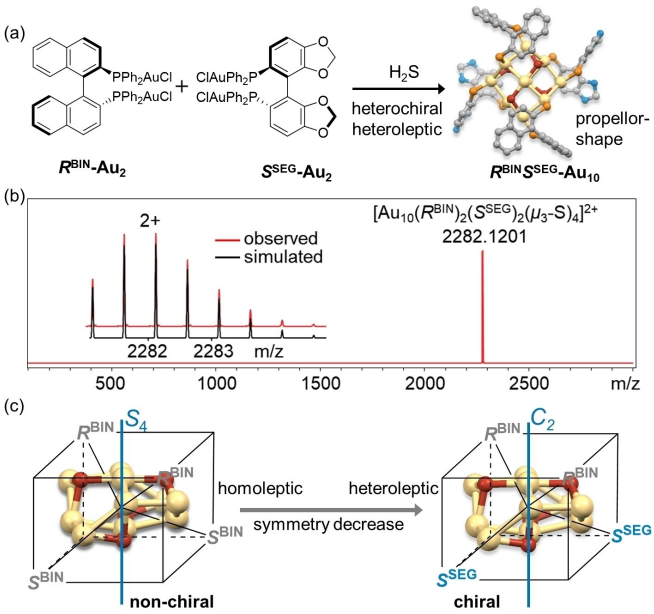

Figure 3. (a) Synthetic route and crystal structure of heteroleptic chiral cluster $R^{BIN}S^{SEG}$-Au_{10}. (The counter-anions, hydrogen atoms, and phenyl rings are omitted for clarity. Au, yellow; S, red; P, orange; C, grey; O, blue.) (b) High resolution ESI-TOF mass spectrum of $R^{BIN}S^{SEG}$-Au_{10} with the inset showing the observed and simulated isotopic patterns of dicationic cluster ion. (c) Illustration of the symmetry lowering from non-chiral ***meso***^{BIN}-Au_{10} to chiral heteroleptic $R^{BIN}S^{SEG}$-Au_{10}.

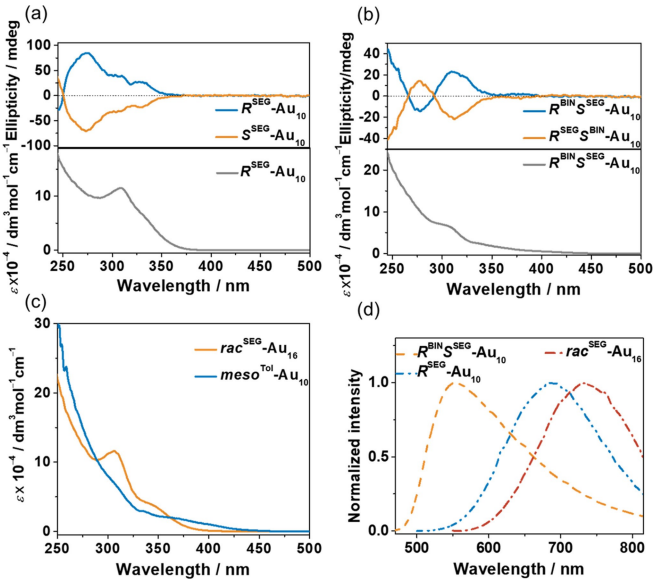

Figure 4. (a) UV/Vis spectrum of R^{SEG}-Au_{10} and CD spectra of R^{SEG}-Au_{10} and S^{SEG}-Au_{10}. (b) UV/Vis spectra of ***rac***^{SEG}-Au_{16} and ***meso***^{Tol}-Au_{10}. (c) UV/Vis spectrum of $R^{BIN}S^{SEG}$-Au_{10} and CD spectra of $R^{BIN}S^{SEG}$-Au_{10} and $R^{SEG}S^{BIN}$-Au_{10}. (d) Normalized emission spectra of $R^{BIN}S^{SEG}$-Au_{10}, R^{SEG}-Au_{10}, and ***rac***^{SEG}-Au_{16} in the solid state.

SEGPHOS ligands with opposite chirality have dominated the assembly process. This represents the first report on the isolation of chiral gold(I)-sulfido complexes with both heterochiral and heteroleptic ligands.

To uncover the optimal and thermodynamic nature of the propellor-shape Au_{10} structure, heterochiral and heteroleptic self-sorting between SEGPHOS and Tol-BINAP as well as BINAP and Tol-BINAP ligands with opposite chirality have been studied by employing the respective chiral chlorogold(I) precursors. As expected, a series of heteroleptic chiral Au_{10} clusters, $R^{SEG}S^{Tol}$-Au_{10}, $R^{Tol}S^{SEG}$-Au_{10}, $R^{BIN}S^{Tol}$-Au_{10}, and $R^{Tol}S^{BIN}$-Au_{10}, was successfully obtained through similar synthetic approach. ESI-MS analysis clearly identifies the formation of heteroleptic Au_{10} complexes (Figures S10–S13). Similarly, $R^{BIN}S^{Tol}$-Au_{10} crystallizes in chiral space group $P2_12_12$ and its crystal structure reveals the adoption of the propellor-shape Au_{10} structure (Figure S14). Therefore, the propellor-shape Au_{10} structure is supposed to be more thermodynamically stable than the four-leaf-clover-shape Au_{10} structure, and heterochiral and heteroleptic self-discrimination probably occurs prior to homochiral self-recognition in this chiral cluster system.

The four-leaf-clover-shape Au_{10} complexes absorb UV light with wavelengths of less than 400 nm, giving rise to colorless solutions. R^{SEG}-Au_{10} and S^{SEG}-Au_{10} show absorption maxima at around 309 nm with a shoulder at *ca.* 332 nm (Figure 4a). Even though ***rac***^{SEG}-Au_{16} possesses a high nuclearity cluster structure, absorption bands in the UV region at *ca.* 306 and 343 (sh) are observed (Figure 4b). The relatively open structure with less extensive Au(I)···Au(I) interactions is probably responsible for the absorption of UV light for ***rac***^{SEG}-Au_{16}. In accordance with BINAP-based Au_{10} complexes, R^{Tol}-Au_{10} and S^{Tol}-Au_{10} have an absorption shoulder at about 337 nm (Figure S15). In contrast, the solutions and crystalline solids of propellor-shape Au_{10} complexes (***meso***^{Tol}-Au_{10}, $R^{SEG}S^{BIN}$-Au_{10}, $R^{BIN}S^{SEG}$-Au_{10}, $R^{SEG}S^{Tol}$-Au_{10}, $R^{Tol}S^{SEG}$-Au_{10}, $R^{BIN}S^{Tol}$-Au_{10}, and $R^{Tol}S^{BIN}$-Au_{10}) are both yellow in color with an absorption tail in the visible region from 400 to 450 nm in the UV/Vis spectrum (Figures 4b, c, S16 and S17). The above results clearly indicate that their photophysical properties are different and are highly dependent on their structural patterns.

The chiral configurations of polynuclear gold(I) complexes have been explored by CD analysis. The CD spectra of R^{SEG}-Au_{10}, S^{SEG}-Au_{10}, R^{Tol}-Au_{10}, and S^{Tol}-Au_{10} display intense Cotton effects and a mirror image relationship in the range of 250–380 nm (Figures 4a and S15). For the heteroleptic propellor-shape Au_{10} clusters, the Cotton effects and mirror image relationship between enantiomers are found to locate in the region of 250–400 nm, corresponding to their UV/Vis absorption (Figures 4b, S16, and S17). The CD spectra confirm the chiral nature of these heteroleptic propellor-shape Au_{10} clusters (Figures 4b, S16, and S17). The butterfly-shape chiral Au_{16} is crystallized as a racemic mixture and is CD-silent in the CD spectra.

In order to further elucidate the origin of chirality in the chiral gold(I) sulfido clusters, we have evaluated the Hausdorff chirality measure[67,68] (HCM, see the Supporting Information) values for both the clusters and their constituent fragments (Au–S core and chiral ligands). The HCM value serves to quantify the degree of overlap between a given moiety and its mirror image. Our findings demonstrate that the HCM values for Au–S cores of $R^{BIN}S^{SEG}$-Au_{10} and

$R^{BIN}S^{Tol}$-Au_{10} are relatively small (Table 1), thereby suggesting a negligible contribution to overall chirality. The primary source of chirality stems from the spatial arrangement of the chiral ligands. This observation is corroborated by the comparatively weak CD signal exhibited by $R^{BIN}S^{Tol}$-Au_{10} (Figure S17), which aligns with its possession of the smallest overall HCM value among the four clusters under investigation. In contrast, both the Au–S core (HCM > 0.1) and the peripheral ligand environment (HCM ≈ 0.11) significantly contribute to the overall chirality in S^{SEG}-Au_{10} and rac^{SEG}-Au_{16}.

These newly formed gold(I) complexes emit weakly in solution. Therefore, only solid-state emissions are reported here. According to previous reports, the low-energy emission bands at around 600–800 nm are tentatively assigned as triplet ligand-to-metal charge transfer excited state (^{3}LMCT) modified by metal···metal interactions or alternatively from the triplet ligand-to-metal – metal charge transfer (^{3}LMMCT) excited state, while the high-energy emission maxima in the range of 500–600 nm are assigned as triplet metal-perturbed intraligand (^{3}IL) phosphorescence (Figure 4d).[30,31,33] Their lifetimes in microsecond range confirm the phosphorescence nature of the emissions (Table S7).[30,31,33] The heteroleptic Au_{10} clusters, $R^{BIN}S^{SEG}$-Au_{10} and $R^{SEG}S^{BIN}$-Au_{10}, show the highest photoluminescence quantum yields of 6.5 % and 6.8 % in this system (Table S7), probably attributed to the rather rigid and compact cluster structure with shorter Au(I)···Au(I) interactions in this system (Tables S4 and S5). The structure and symmetry as well as Au(I)···Au(I) interactions of the gold(I)-sulfido complexes are obviously influenced by altering combinations of the chiral ligands, leading to different photophysical behaviors and emission origins.

Besides the employment of heteroleptic precursors with opposite chirality, attempts have been made to construct the heteroleptic chiral Au_{10} complexes from cluster-to-cluster transformation. Equal equivalents of R^{BIN}-Au_{10} and S^{SEG}-Au_{10} were stirred in DCM under reflux for 2 h (Figure 5a). The UV/Vis spectrum shows an absorbance growth in the range of 354–425 nm and an absorbance drop at the maxima of around 310 and 330 nm. These together with CD spectral changes indicate the formation of a propellor-shape Au_{10} cluster, $R^{BIN}S^{SEG}$-Au_{10} (Figures 5b, c, and S18). Further evidence came from the ESI-MS studies. By mixing R^{BIN}-Au_{10} and S^{SEG}-Au_{10} at room temperature (r.t.) for 24 h, an incomplete cluster-to-cluster transformation occurs with the coexistence of Au_{10} clusters with ligand combinations of $(S^{SEG})_4$, $(S^{SEG})_3(R^{BIN})$, $(S^{SEG})_2(R^{BIN})_2$, $(S^{SEG})(R^{BIN})_3$, and $(R^{BIN})_4$ (Figure 5d). Time-dependent ESI-MS analysis demonstrates that this cluster-to-cluster transformation is accelerated under heating and the majority of Au_{10} clusters is converted to heterochiral and heteroleptic $R^{BIN}S^{SEG}$-Au_{10} ($(R^{SEG})_2(S^{BIN})_2$) upon heating at 50 °C after 6 h (Figures 5d and S19). In other words, the four-leaf-clover-shape Au_{10} mixture of R^{BIN}-Au_{10} and S^{SEG}-Au_{10} undergoes a heterochiral and heteroleptic self-sorting and a structure rearrangement in solution, leading to the formation of the propellor-shape heteroleptic Au_{10}.

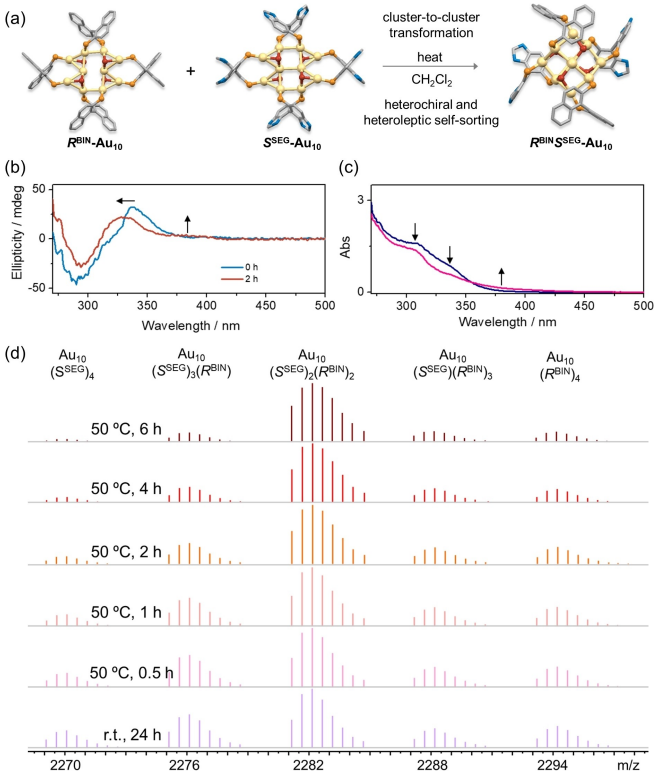

Figure 5. (a) Schematic illustration showing the cluster-to-cluster transformation from R^{BIN}-Au_{10} and S^{SEG}-Au_{10} to $R^{BIN}S^{SEG}$-Au_{10} via heterochiral and heteroleptic self-sorting. (b) CD and (c) UV/Vis spectral changes upon heating the reaction at 50 °C for 2 h. (d) ESI-Mass spectral changes by mixing R^{BIN}-Au_{10} and S^{SEG}-Au_{10} at r.t. for 24 h and upon heating the reaction at 50 °C for 0.5 h, 1 h, 2 h, 4 h, and 6 h.

To further explore the heterochiral and heteroleptic self-sorting phenomenon, we have conducted competition experiments. A mixture of R^{SEG}-Au_{10}, S^{SEG}-Au_{10}, R^{BIN}-Au_{10} and S^{BIN}-Au_{10} in a mole ratio of 1:1:1:1 was stirred under 50 °C for 6 hours (Figure 6). The growth in absorbance at around 400 nm and the absorbance drop at around 310 and 330 nm in the UV/Vis spectra (Figure S20) as well as the isolation of yellow crystals typical of the propellor-shape structure from the reaction mixure (Figure S21) indicate the formation of propellor-shape Au_{10} clusters. The existence of Au_{10} clusters with ligand combinations of $(SEGPHOS)_4$, $(SEGPHOS)_3(BINAP)$, $(SEGPHOS)_2(BINAP)_2$, $(SEGPHOS)(BINAP)_3$, and $(BINAP)_4$ is revealed by ESI-MS analysis. The heteroleptic Au_{10} cluster protected by ligands of $R^{SEG}S^{SEG}R^{BIN}S^{BIN}$ is found to be the principal

Table 1: Hausdorff chirality measure values for S^{SEG}-Au_{10}, $R^{BIN}S^{SEG}$-Au_{10}, $R^{BIN}S^{Tol}$-Au_{10} and rac^{SEG}-Au_{16} at their X-ray crystal structures.

Cluster	Au–S core[a]	Chiral ligands	Total
S^{SEG}-Au_{10}	0.200	0.116	0.116
$R^{BIN}S^{SEG}$-Au_{10}	0.017	0.081	0.080
$R^{BIN}S^{Tol}$-Au_{10}	0.022	0.073	0.073
rac^{SEG}-Au_{16}	0.112	0.108	0.107

[a] $Au_{10}S_4$ for Au_{10} clusters and $Au_{16}S_6$ for rac^{SEG}-Au_{16}.

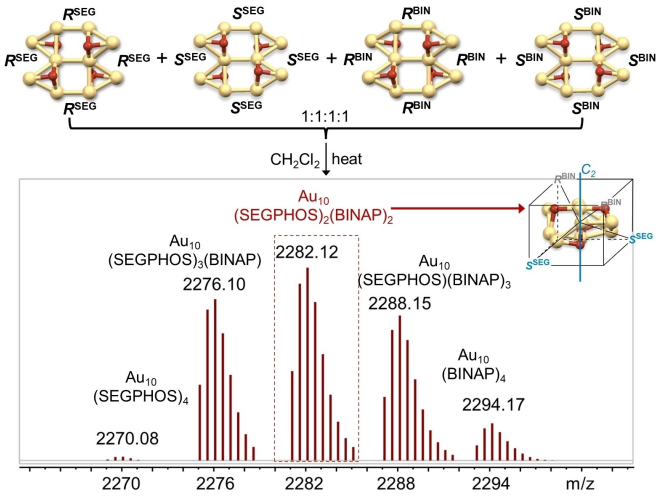

Figure 6. Reaction of R^{SEG}-Au_{10}, S^{SEG}-Au_{10}, R^{BIN}-Au_{10}, and S^{BIN}-Au_{10} in equal equivalents is monitored by ESI-MS.

product (Figure 6). The co-existence of Au_{10} clusters with different ligand compositions proves the facile ligand exchange ability of these propellor-shape Au_{10} clusters in this system. The absence of Au_{16} in this reaction system suggests the formation of propellor-shape Au_{10} cluster is prior to that of SEGPHOS-based butterfly-shape Au_{16} cluster. These results demonstrate that the heterochiral and heteroleptic self-sorting dominates the self-assembly processes in this system.

To explore the full potential of the chiral self-sorting in the chiral gold(I) sulfido cluster system, another type axial chiral spiroketal-based diphosphine ligand ((*S,S,S*)-SKP, S^{SKP})[69,70] protected Au_6 cluster ($[Au_6(S^{SKP})_3(\mu_3\text{-}S)_2](PF_6)_2$, ***S*^{SKP}-Au$_6$**), which was newly synthesized and has been fully characterized (Figures S22–S24), was utilized to react with ***R*^{SEG}-Au$_{10}$** in a mole ratio of 4:3 under 50 °C for 6 hours. Seen from the ESI mass spectra (Figure S25), even though ***R*^{SEG}-Au$_{10}$** and ***S*^{SKP}-Au$_6$** remains to be the principal species in the reaction mixture, the appearance of Au_6 and Au_{10} clusters with respective ligand combinations of $(SKP)_2$-(SEGPHOS) and $(SKP)(SEGPHOS)_3$ still indicate the existence of heterochiral and heteroleptic self-sorting between different types of axial chiral ligands (SKP and SEGPHOS) protected gold(I) sulfido clusters of distinct nuclearity and symmetry. This result could herald the ubiquity of heterochiral and heteroleptic self-sorting in gold(I) cluster system, and open up a new avenue for an exploration to fully uncover the self-sorting behavior in gold(I)-sulfido cluster systems.

Conclusion

In summary, employing different combinations of heterochiral and heteroleptic ligands, novel heteroleptic chiral propellor-shape Au_{10} clusters have been constructed through an unprecedented heterochiral and heteroleptic self-sorting strategy. Compared to the homoleptic *meso* ones, the incorporation of heteroleptic ligands has led to symmetry lowering from S_4 to C_2. The chirality has been transferred from the chiral ligands and stored at the newly formed heteroleptic Au_{10} species. Besides, a unique butterfly-shape chiral Au_{16} complex with different ratios of R^{SEG} and S^{SEG} ligands is obtained via heterochiral self-sorting. The cluster-to-cluster transformation experiments further identify the propellor-shape Au_{10} cluster structures to be the optimal structural pattern in this cluster system. The current work would guide the future design of heteroleptic chiral gold clusters and bi-functional artificial chiral species using mixed-ligand strategy, especially for assembling water-soluble chiral gold clusters with both chiral and hydrophilic hetero-ligands for bimedical applications.[71] Our research may also contribute to a better understanding of the heterochiral and heteroleptic self-sorting and self-assembly processes involved in nature.

Acknowledgements

This work was financially supported by the Key Program of the Major Research Plan on "Architectures, Functionalities and Evolution of Hierarchical Clusters" of the National Natural Science Foundation of China (NSFC 91961202) and a General Research Fund (GRF) from the Research Grants Council of the Hong Kong Special Administrative Region, P. R. China (HKU 17303421). Support from the Innovation Technology Commission (ITC) to the State Key Laboratory of Synthetic Chemistry is acknowledged. The CAS-Croucher Funding Scheme for Joint Laboratories on "Molecular Functional Materials for Electronics, Switching and Sensing" and The University of Hong Kong are also gratefully acknowledged. The Beijing Synchrotron Radiation Facility (BSRF) is acknowledged for providing beamline time for the SCXRD analysis. We also thank the staff of BL17B1 beamline at the National Facility for Protein Science (NFPS) of the Shanghai Synchrotron Radiation Facility (SSRF), Shanghai, People's Republic of China, for assistance during data collection. The instrumental support from the Analysis and Testing Center of Beijing Institute of Technology is also highly appreciated. Prof. Kuiling Ding at Shanghai Institute of Organic Chemistry is warmly thanked for his generous donation of SKP ligand. The computations were performed using research computing facilities offered by Information Technology Services, The University of Hong Kong.

Conflict of Interest

The authors declare no conflict of interest.

Data Availability Statement

The data that support the findings of this study are available in the supplementary material of this article.

Keywords: Chiral Self-Sorting · Cluster-to-Cluster Transformation · Gold(I)-Sulfido Cluster · Heteroleptic Self-Sorting · Luminescence

[1] J. M. Lehn, *Angew. Chem. Int. Ed.* **1988**, *27*, 89–112.
[2] R. Chakrabarty, P. S. Mukherjee, P. J. Stang, *Chem. Rev.* **2011**, *111*, 6810–6918.
[3] M. Fujita, *Chem. Soc. Rev.* **1998**, *27*, 417–425.
[4] M. M. Safont-Sempere, G. Fernández, F. Würthner, *Chem. Rev.* **2011**, *111*, 5784–5814.
[5] A. Scarso, J. Jr. Rebek, *Top. Curr. Chem.* **2006**, *265*, 1–46.
[6] M. Liu, L. Zhang, T. Wang, *Chem. Rev.* **2015**, *115*, 7304–7397.
[7] H. Jędrzejewska, A. Szumna, *Chem. Rev.* **2017**, *117*, 4863–4899.
[8] Y.-Q. Zou, D. Zhang, T. K. Ronson, A. Tarzia, Z. Lu, K. E. Jelfs, J. R. Nitschke, *J. Am. Chem. Soc.* **2021**, *143*, 9009–9015.
[9] H. Yamagishi, T. Fukino, D. Hashizume, T. Mori, Y. Inoue, T. Hikima, M. Takata, T. Aida, *J. Am. Chem. Soc.* **2015**, *137*, 7628–7631.
[10] D. M. Engelhard, J. Nowack, G. H. Clever, *Angew. Chem. Int. Ed.* **2017**, *56*, 11640–11644.
[11] H. Jędrzejewska, M. Wierzbicki, P. Cmoch, K. Rissanen, A. Szumna, *Angew. Chem. Int. Ed.* **2014**, *53*, 13760–13764.
[12] W. Makiguchi, J. Tanabe, H. Yamada, H. Iida, D. Taura, N. Ousaka, E. Yashima, *Nat. Commun.* **2015**, *6*, 7236.
[13] C. Gütz, R. Hovorka, N. Struch, J. Bunzen, G. Meyer-Eppler, Z.-W. Qu, S. Grimme, F. Topić, K. Rissanen, M. Cetina, M. Engeser, A. Lützen, *J. Am. Chem. Soc.* **2014**, *136*, 11830–11838.
[14] C. G. Claessens, T. Torres, *J. Am. Chem. Soc.* **2002**, *124*, 14522–14523.
[15] A. X. Wu, A. Chakraborty, J. C. Fettinger, R. A. Flowers, L. M Isaacs, *Angew. Chem. Int. Ed.* **2002**, *41*, 4028–4031.
[16] T. Tateishi, T. Kojima, S. Hiraoka, *Commun. Chem.* **2018**, *1*, 20.
[17] P. Wagner, F. Rominger, W.-S. Zhang, J. H. Gross, S. M. Elbert, R. R. Schröder, M. Mastalerz, *Angew. Chem. Int. Ed.* **2021**, *60*, 8896–8904.
[18] K. Tamura, P. Schimmel, *Science* **2004**, *305*, 1253.
[19] K. Tamura, P. R. Schimmel, *Proc. Natl. Acad. Sci. USA* **2006**, *103*, 13750–13752.
[20] R. Wolfenden, *Chem. Rev.* **2006**, *106*, 3379–3396.
[21] A. Radzicka, R. Wolfenden, *Science* **1995**, *267*, 90–93.
[22] A. Calcaterra, I. D'Acquarica, *J. Pharm. Biomed. Anal.* **2018**, *147*, 323–340.
[23] T. Andersson, L. Weidolf, *Clin. Drug Invest.* **2008**, *28*, 263–279.
[24] H. Schmidbaur, A. Schier, *Chem. Soc. Rev.* **2012**, *41*, 370–412.
[25] C.-M. Che, S.-W. Lai, *Coord. Chem. Rev.* **2005**, *249*, 1296–1309.
[26] V. W.-W. Yam, V. K.-M. Au, S. Y.-L. Leung, *Chem. Rev.* **2015**, *115*, 7589–7728.
[27] M. C. Gimeno, A. Laguna, *Chem. Soc. Rev.* **2008**, *37*, 1952–1966.
[28] R. J. Puddephatt, *Chem. Soc. Rev.* **2008**, *37*, 2012–2027.
[29] V. W.-W. Yam, E. C.-C. Cheng, *Chem. Soc. Rev.* **2008**, *37*, 1806–1813.
[30] V. W.-W. Yam, E. C.-C. Cheng, K.-K. Cheung, *Angew. Chem. Int. Ed.* **1999**, *38*, 197–199.
[31] V. W.-W. Yam, E. C.-C. Cheng, Z.-Y. Zhou, *Angew. Chem. Int. Ed.* **2000**, *39*, 1683–1685.
[32] D. Fenske, T. Langetepe, M. M. Kappes, O. Hampe, P. Weis, *Angew. Chem. Int. Ed.* **2000**, *39*, 1857–1860.
[33] V. W.-W. Yam, E. C.-C. Cheng, N. Zhu, *Angew. Chem. Int. Ed.* **2001**, *40*, 1763–1765.
[34] T. K.-M. Lee, N. Zhu, V. W.-W. Yam, *J. Am. Chem. Soc.* **2010**, *132*, 17646–17648.
[35] L.-Y. Yao, F. K.-W. Hau, V. W.-W. Yam, *J. Am. Chem. Soc.* **2014**, *136*, 10801–10806.
[36] F. K.-W. Hau, T. K.-M. Lee, E. C.-C. Cheng, V. K.-M. Au, V. W.-W. Yam, *Proc. Natl. Acad. Sci. USA* **2014**, *111*, 15900–15905.
[37] X.-L. Pei, Y. Yang, Z. Lei, S.-S. Chang, Z.-J. Guan, X.-K. Wan, T.-B. Wen, Q.-M. Wang, *J. Am. Chem. Soc.* **2015**, *137*, 5520–5525.
[38] L.-Y. Yao, V. W.-W. Yam, *J. Am. Chem. Soc.* **2015**, *137*, 3506–3509.
[39] L.-Y. Yao, T. K.-M. Lee, V. W.-W. Yam, *J. Am. Chem. Soc.* **2016**, *138*, 7260–7263.
[40] A. Chu, F. K.-W. Hau, L.-Y. Yao, V. W.-W. Yam, *ACS Materials Lett.* **2019**, *1*, 277–284.
[41] L.-Y. Yao, K.-H. Low, V. W.-W. Yam, *Chem* **2019**, *5*, 2418–2428.
[42] L.-L. Yan, L.-Y. Yao, V. W.-W. Yam, *J. Am. Chem. Soc.* **2020**, *142*, 11560–11568.
[43] L.-Y. Yao, Z. Chen, K. Zhang, V. W.-W. Yam, *Angew. Chem. Int. Ed.* **2020**, *59*, 21163–21169.
[44] L.-Y. Yao, V. W.-W. Yam, *J. Am. Chem. Soc.* **2021**, *143*, 2558–2566.
[45] L.-L. Yan, L.-Y. Yao, M. Ng, V. W.-W. Yam, *J. Am. Chem. Soc.* **2021**, *143*, 19008–19017.
[46] S.-S. Zhang, L. Feng, R. D. Senanayake, C. M. Aikens, X.-P. Wang, Q.-Q. Zhao, C.-H. Tung, D. Sun, *Chem. Sci.* **2018**, *9*, 1251–1258.
[47] S. Zhang, Y. Li, L. Feng, Q. Xue, Z. Gao, C.-H. Tung, D. Sun, *Nano Res.* **2021**, *14*, 3343–3351.
[48] S.-K. Yip, E. C.-C. Cheng, L.-H. Yuan, N. Zhu, V. W.-W. Yam, *Angew. Chem. Int. Ed.* **2004**, *43*, 4954–4957.
[49] S.-Y. Yu, Z.-X. Zhang, E. C.-C. Cheng, Y.-Z. Li, V. W.-W. Yam, H.-P. Huang, R.-B. Zhang, *J. Am. Chem. Soc.* **2005**, *127*, 17994–17995.
[50] P. Sevillano, O. Fuhr, M. Kattannek, P. Nava, O. Hampe, S. Lebedkin, R. Ahlrichs, D. Fenske, M. M. Kappes, *Angew. Chem. Int. Ed.* **2006**, *45*, 3702–3708.
[51] S.-Y. Yu, Q.-F. Sun, T. K.-M. Lee, E. C.-C. Cheng, Y.-Z. Li, V. W.-W. Yam, *Angew. Chem. Int. Ed.* **2008**, *47*, 4551–4554.
[52] G. F. Manbeck, W. W. Brennessel, R. A. Stockland, R. Eisenberg, *J. Am. Chem. Soc.* **2010**, *132*, 12307–12318.
[53] I. O. Koshevoy, Y. C. Chang, A. J. Karttunen, M. Haukka, T. Pakkanen, P.-T. Chou, *J. Am. Chem. Soc.* **2012**, *134*, 6564–6567.
[54] W.-X. Ni, M. Li, J. Zheng, S.-Z. Zhan, Y.-M. Qiu, S.-W. Ng, D. Li, *Angew. Chem. Int. Ed.* **2013**, *52*, 13472–13476.
[55] X.-F. Jiang, F. K.-W. Hau, Q.-F. Sun, S.-Y. Yu, V. W.-W. Yam, *J. Am. Chem. Soc.* **2014**, *136*, 10921–10929.
[56] Z. Lei, X.-L. Pei, Z.-G. Jiang, Q.-M. Wang, *Angew. Chem. Int. Ed.* **2014**, *53*, 12771–12775.
[57] D. Y. Melgarejo, G. M. Chiarella Jr., J. P. Fackler, *Inorg. Chem.* **2016**, *55*, 11883–11889.
[58] J. Braese, A. Schinabeck, M. Bodensteiner, H. Yersin, A. Y. Timoshkin, M. Scheer, *Chem. Eur. J.* **2018**, *24*, 10073–10077.
[59] M. Jin, T. Sumitani, H. Sato, T. Seki, H. Ito, *J. Am. Chem. Soc.* **2018**, *140*, 2875–2879.
[60] D. T. Walters, R. B. Aghakhanpour, X. B. Powers, K. B. Ghiassi, M. M. Olmstead, A. L. Balch, *J. Am. Chem. Soc.* **2018**, *140*, 7533–7542.
[61] G.-T. Xu, L.-L. Wu, X.-Y. Chang, T. W.-H. Ang, W.-Y. Wong, J.-S. Huang, C.-M. Che, *Angew. Chem. Int. Ed.* **2019**, *58*, 16297–16306.
[62] X.-L. Pei, P. Zhao, H. Ube, Z. Lei, K. Nagata, M. Ehara, M. Shionoya, *J. Am. Chem. Soc.* **2022**, *144*, 2156–2163.
[63] K. Wu, J. Tessarolo, A. Baksi, G. H. Clever, *Angew. Chem. Int. Ed.* **2022**, *61*, e202205725.
[64] J. Tessarolo, H. Lee, E. Sakuda, K. Umakoshi, G. H. Clever, *J. Am. Chem. Soc.* **2021**, *143*, 6339–6344.

[65] R. P. Herrera, M. C. Gimeno, *Chem. Rev.* **2021**, *121*, 8311–8363.
[66] M.-M. Zhang, K. Li, S.-Q. Zang, *Adv. Opt. Mater.* **2020**, *8*, 1902152.
[67] A. B. Buda, K. Mislow, *J. Am. Chem. Soc.* **1992**, *114*, 6006–6012.
[68] I. L. Garzón, M. R. Beltrán, G. González, I. Gutıerrez-González, K. Michaelian, J. A. Reyes-Nava, J. I. Rodrıguez-Hernández, *Eur. Phys. J. D* **2003**, *24*, 105–109.
[69] X. Wang, Z. Han, Z. Wang, K. Ding, *Acc. Chem. Res.* **2021**, *54*, 668–684.
[70] Z.-Y Cao, X. Wang, C. Tan, X.-L. Zhao, J. Zhou, K. Ding, *J. Am. Chem. Soc.* **2013**, *135*, 8197–8200.
[71] H. Ajioka, M. Komada, H. Yao, *Phys. Chem. Chem. Phys.* **2022**, *24*, 29223–29231.
[72] Deposition numbers 2221327 (for $\boldsymbol{R}^{\mathbf{BIN}}\boldsymbol{S}^{\mathbf{SEG}}$-$\mathbf{Au_{10}}$), 2221328 (for $\boldsymbol{R}^{\mathbf{SEG}}\boldsymbol{S}^{\mathbf{BIN}}$-$\mathbf{Au_{10}}$), 2221329 (for $\boldsymbol{R}^{\mathbf{BIN}}\boldsymbol{S}^{\mathbf{Tol}}$-$\mathbf{Au_{10}}$), 2221330 (for ***rac***$^{\mathbf{SEG}}$-$\mathbf{Au_{16}}$), 2221331 (for ***meso***$^{\mathbf{Tol}}$-$\mathbf{Au_{10}}$), 2221332 (for $\boldsymbol{S}^{\mathbf{SEG}}$-$\mathbf{Au_{10}}$) contain the supplementary crystallographic data for this paper. These data are provided free of charge by the joint Cambridge Crystallographic Data Centre and Fachinformationszentrum Karlsruhe Access Structures service.

Manuscript received: October 26, 2023
Accepted manuscript online: November 27, 2023
Version of record online: December 14, 2023